

CFD APPLICATIONS AT PALMER NICKEL AND COBALT REFINERY

Peter Allen¹, Matthew White¹, Ross Haywood^{1*} (HATCH)
Bill Anderson², Rohan O'Farrell², and Russell Hobson², (PNCR)

¹ Hatch, 61 Petrie Terrace, Brisbane Australia

² Palmer Nickel and Cobalt Refinery, Townsville

*Corresponding author E-mail address: rhaywood@hatch.com.au

ABSTRACT

Being successful in the industrial application of computational fluid dynamic (CFD) modelling requires the ability to find a suitable balance between academic rigour and real-world expediency. Two case studies encountered at the Palmer Nickel and Cobalt Refinery (PNCR) are presented in this paper. The first involves the analysis of a mixing vessel, while the second includes an investigation of a hot gas generator. Both studies contain complex systems, for which relatively simple CFD models have been developed. Exclusion of physical phenomena irrelevant to the key design and operating considerations has allowed the CFD models to answer important questions quickly and at low cost.

NOMENCLATURE

| | |
|--------|--|
| N | Impeller Speed (rev/s) |
| N_p | Impeller Power Number |
| N_Q | Flow Number |
| τ | Torque (Nm) |
| ρ | Density (kg/m^3) |
| π | Pi |
| D | Diameter (m) |
| Q | Volumetric Flow Rate (m^3/s) |
| D_T | Tank Diameter (mm) |
| D_A | Impeller Diameter (mm) |

CASE STUDY 1 – SLURRY TANK

PNCR identified that the addition of concentrated sulphuric acid to the cobalt-sulphide slurry mixing tank in the atmospheric leaching stage of the plant had the effect of shortening the leaching reaction time, allowing greater production rates to be achieved through this stage of processing. During trials of this means of acid addition, excessive localised failure was found on the tank walls and roof from accelerated corrosion. On inspection, this was traced to the location of the acid injection point and a CFD analysis of the tank was undertaken to try to understand the problem and determine a possible solution.

Model Description – Validation Case

The first step in modelling the mixing vessel was validation of the proposed CFD modelling technique such

that the results ultimately obtained could be used with confidence. The experimental results of Weetman and Salzman 1981, were used for this step of model validation. Their experiment (as shown in Figure 1) consisted of a single commercially available axial flow gas-liquid dispersion impeller in a cylindrical, flat-bottomed vessel with four equally spaced baffles. Although a different physical size, this physical setup had all of the features of the prototype system at PNCR.

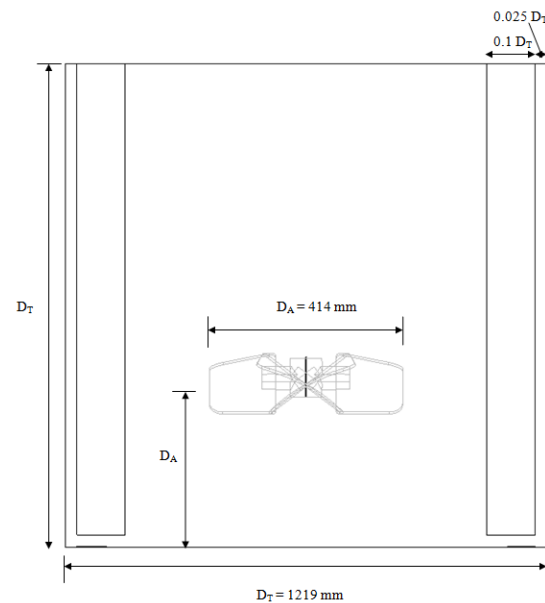


Figure 1: Experimental Vessel Geometry

A 3D CAD geometry of the vessel CFD volume was generated using Solid Edge™ modelling software and imported into ANSYS Workbench. To adopt a Multiple Reference Frame (MRF) approach to modelling the rotating impeller, a mesh was generated within two separate (but connected) domains for the main vessel and a volume containing the impeller geometry. The native CFX meshing package was used to develop an unstructured tetrahedral mesh in both domains due to the complex geometry around the impeller blades and the lack of a well defined or preferential flow direction generally. Inflation layers were applied to all wall surfaces to capture boundary layer effects. An example of the mesh generated for the validation model is shown in Figure 2.

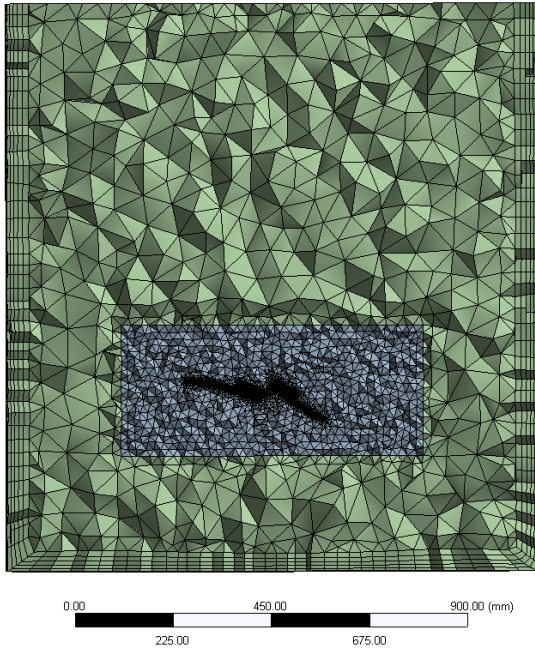


Figure 2: Computational mesh used for model validation

The main considerations in meshing of mixing vessels for CFX were:

- A simplified, “clean” geometry of the CFD volume
- Separate domains for each of the stationary (tank) and rotating (impeller) domains.
- Correctly sized inflation layers on all wall boundaries
- Refinement of mesh sizing around the impeller
- Matching mesh sizing on either side of domain boundaries
- A General Grid Interface (GGI) for the interface between domains so that matching grids were unnecessary.
- Mesh orthogonal quality greater than 0.1

The mesh was imported into the ANSYS CFX pre-processor to set up boundary conditions and apply physical models.

Classically there are two approaches to modelling the rotating impeller present in mixing vessels: i) a sliding mesh transient simulation or ii) a multiple reference frame (MRF) steady-state simulation. The former has been used extensively in simulations of mixing vessels and involves computationally rotating the mesh containing the impeller geometry. This in turn requires the mesh to be “solved” for each iteration and solution convergence for each transient time-step. This can provide a very accurate result and will reveal any transient effects associated with local blade passage. However, the need to resolve the mesh and fluid flow for each time-step makes it computationally intensive.

The simpler approach, using MRF (one each for the tank and impeller) with a suitable averaging across the inter-domain interface allows for a single steady-state simulation within the combined domains. This approach does not require mesh rotation at each iteration. This simulation method leads to a time-averaged solution which, while it cannot show transient effects of the flow, provides a reasonable approximation of the overall flow generated by the particular impeller geometry in steady state. The main benefit of this method is the reduction in solver time – typically an order of magnitude. In this model, the transient flow fields were not important and therefore an MRF simulation was adopted.

The relevant domain, boundary conditions and physics models are shown in Table 1

| Domain | Motion | Speed |
|------------------|---------------|--------|
| Impeller Domain | Rotating | 190RPM |
| Vessel Domain | Stationary | - |
| Boundary | Condition | Value |
| Walls | No Slip | Smooth |
| Free Surface | Free Slip | - |
| Domain Interface | Frozen Rotor | GGI |
| Physics | Model | Option |
| Turbulence | RNG k-Epsilon | - |
| Heat Transfer | Isothermal | 25°C |

Table 1: Model Domain, boundary condition and physics models

The material used in this model was water at room temperature and pressure.

The experimental results to be compared included the impeller power, power number, and flow number, as well as velocity vectors in a vertical plane cut through the vessel.

The impeller power is related directly to the torque on the impeller and its rotational speed can be measured experimentally by the power output of the drive motor. From the CFD results, the power (Watts) is calculated by:

$$P = 2 \pi \tau N$$

The power number (N_p) and flow number (N_Q) are dimensionless numbers widely used for the comparison of impellers (Oldshue, 1983, Atiema-Obeng et al., 2004). They are calculated using the power, impeller diameter, speed, and the volumetric flow rate from the impeller:

$$N_p = \frac{P}{\rho N^3 D^5}$$

$$N_Q = \frac{Q}{ND^3}$$

Results – Validation Case

The mixing vessel validation model CFD results were compared to those obtained experimentally. The general nature of the flow is shown in the velocity contour plot (Figure 3). It can be seen from the power and flow

numbers (Table 2) that there is good overall agreement between model and experiment. The vector plots, Figure 4 show the flow vectors are very similar between the experiment and CFD results with similar directions and magnitude at three heights through the vessel.

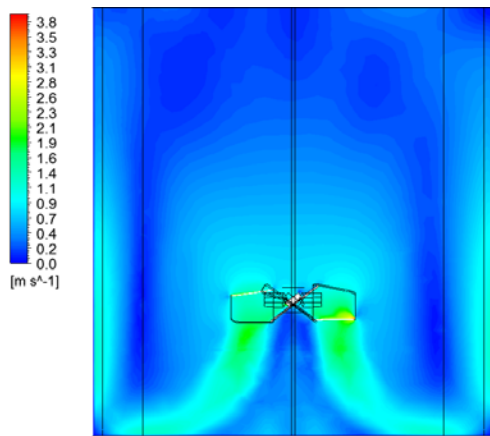


Figure 3: Validation Model velocity contours on vertical Plane

| Variable | CFD Results | Experimental Results |
|-------------|-------------|----------------------|
| Torque (Nm) | 14.78 | - |
| Power (W) | 294 | 290 |
| N_p (-) | 0.76 | 0.73 |
| N_Q (-) | 0.73 | 0.78 |

Table 2: Comparison of CFD and Experimental results for Validation model.

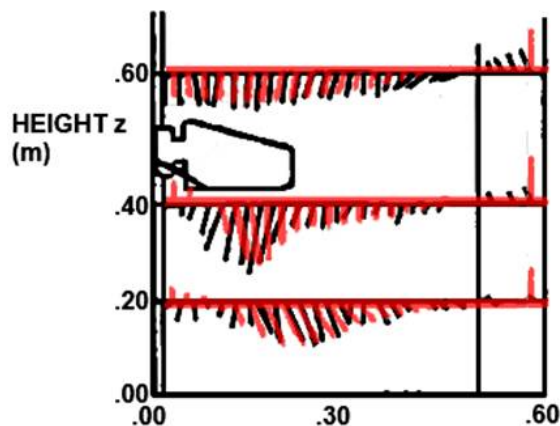


Figure 4: Velocity Vectors. Experimental (black) with CFD results overlaid (red)

Results – PNCr mixing vessel

The resulting methods from the validation process were applied to the PNCr mixing vessel to determine the fluid flows and acid paths/mixing. The setup of this vessel required a slightly more detailed geometry containing extra internals within the vessel. The mixing vessel in this case was 4600mm in height, 2500mm diameter with a 1041mm diameter 6-bladed Rushton impeller and 4 equi-spaced baffles. In this case, there was also a slurry inlet

tube, acid injection point, and an overflow outlet pipe. The resulting CFD volume is shown in Figure 5.

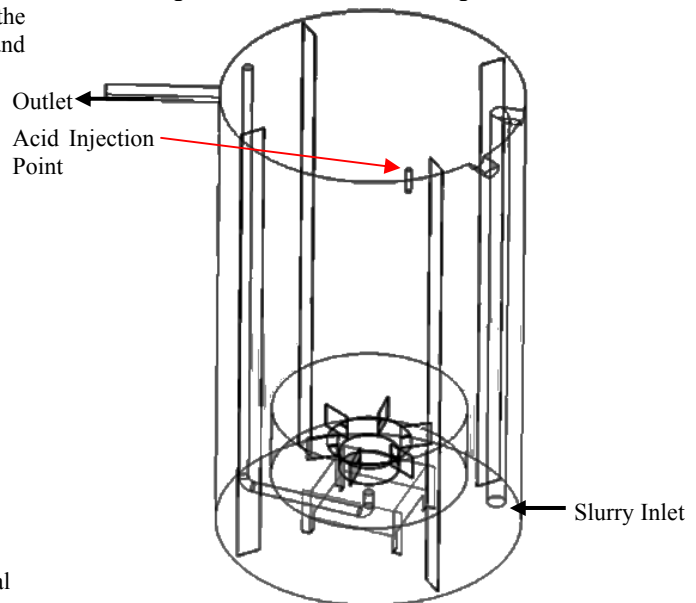


Figure 5: PNCr Mixing Vessel CFD Volume

The same meshing methods and setup methods were used as for the validation model but with two inlets and the outlet added. The materials in this case were a mixture of Cobalt Sulphide slurry and concentrated Sulphuric Acid. The materials, subdomain settings, boundary conditions and physical models used are shown in Table 3.

| Material | Cobalt Sulphide Slurry | H ₂ SO ₄ |
|--------------------------------|------------------------|--------------------------------|
| Viscosity (cP) | 7/2 | 18 |
| % solids (wt%) | 12-13.1 | - |
| Density(kg/m ³) | 1080. | 1826. |
| Temperature(°C) | 110/80 | 70/30 |
| pH (-) | 6-8 | - |
| Concentration | - | 98% |
| Subdomains | | |
| Impeller Domain | Rotating | 128RPM |
| Vessel Domain | Stationary | - |
| Boundary BC Type Value | | |
| Walls | No Slip | Smooth |
| Free Surface | Free Slip | |
| Domain Interface | Frozen Rotor | |
| Slurry Inlet | Mass Flow Inlet | 1.795kg/s |
| Acid Inlet | Mass Flow Inlet | 0.046kg/s |
| Outlet | Pressure Outlet | 1atm |
| Physics Model Option | | |
| Buoyancy | Buoyant | Normal Gravity |
| Turbulence | SST | Curvature Correction |
| Heat Transfer | Isothermal | 80°C |
| Cobalt Sulphide | - | Constraint |
| H ₂ SO ₄ | - | Transport Equation |

Table 3: Materials, Boundary Conditions and Physics

The results of this model were analysed and compared to the site pictures showing areas of excessive corrosion and wall failure to determine whether the acid mixing behaviour was responsible. The site pictures (shown in Figure 6 and Figure 7) indicate the acid inlet location as well as distinct areas of the vessel where corrosion is occurring.



Figure 6: PNCr Mixing Vessel – Acid Inlet and Corrosion



Figure 7: PNCr Mixing Vessel – Inner Wall Corrosion

The following results are from the base case model of the PNCr mixing vessel. In this case, the acid injection point was positioned directly behind a baffle on the leeward side (according to the prevailing background flow). As can be seen in Figure 8 (streamlines of injected acid), Figure 9 (acid mass fraction adjacent to the wall) and Figure 10 (velocity contours on a horizontal plane coincident with the injection point), the acid tends to remain in this area for a prolonged period and mixes only slowly with the background flow. Site observations show that the problem corrosion region corresponded directly with the area in question. Therefore, it was decided to move the inlet to an region with stronger background flow to increase the speed of mixing of the acid into the slurry and, if possible, to an area with less tendency for the direct contact of acid with the vessel walls.



Figure 8: PNCr Vessel, Base-case, Acid Streamlines

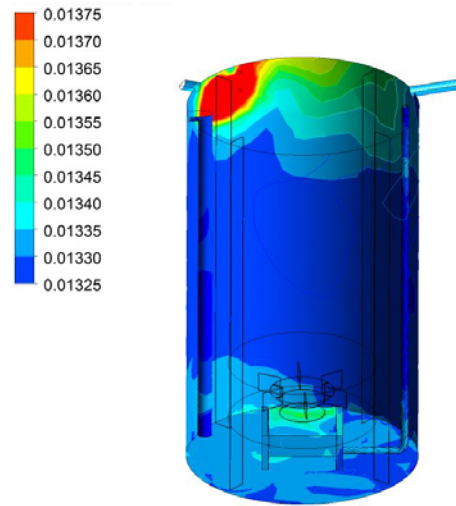


Figure 9: PNCr Vessel Base Case (Acid Mass Fraction on Walls)

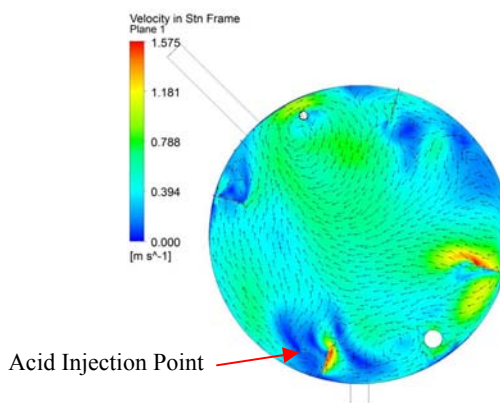


Figure 10: PNCr Vessel Base Case Injection Height Velocity Contours and Vectors

Based on a proposal by site personnel, a second case (Modification 1) was subsequently investigated. The concept was to relocate the acid injection point closer to the centre of the vessel. The results are shown in Figure 11 and, while the acid was found to mix more quickly as desired, the computations suggested that the flow was

directed towards the wall of the vessel, which would be expected again to result in excessive corrosion.

A simple approach was devised to determine a better acid inlet location, based on the tracking of streamlines of the background slurry flow originating from 8 discrete locations near the liquid top surface (as shown in Figure 12). Thus, it was possible to determine quickly a location for injection that would allow a rapid mixing in conjunction with a longer mixing time prior to contact with the walls. The streamlines are shown in Figure 13.

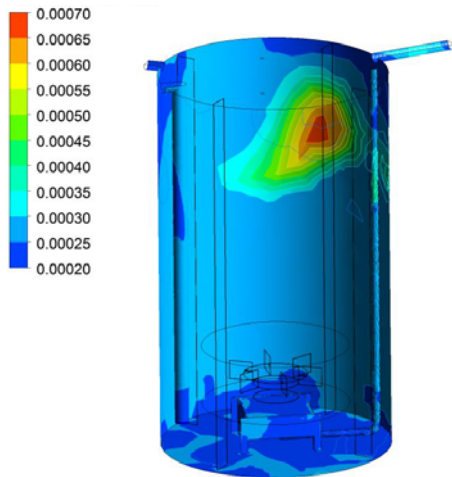


Figure 11: PNCr Modification 1 Acid MF on Walls

On this basis, Point 6 was chosen as the most promising and a full analysis including acid injection was performed. The results are shown in Figure 14 and Figure 15. It can be seen that the acid mixes well down the middle of the vessel and has minimal contact with the tank walls. This configuration was chosen for the site modification of the acid injection system.

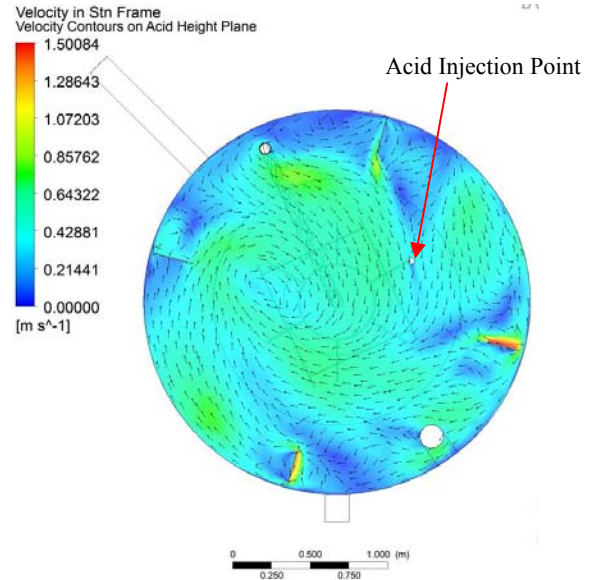


Figure 14: PNCr Vessel Recommended Inlet Location Velocity Contours and Vectors at Injection Height

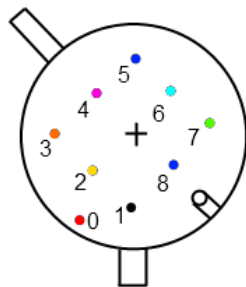


Figure 12: PNCr Vessels Streamline Legend

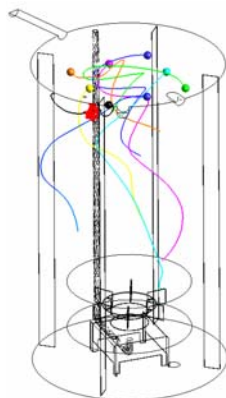


Figure 13: PNCr Vessel Fluid Streamlines originating from 8 distinct locations at the fluid top surface

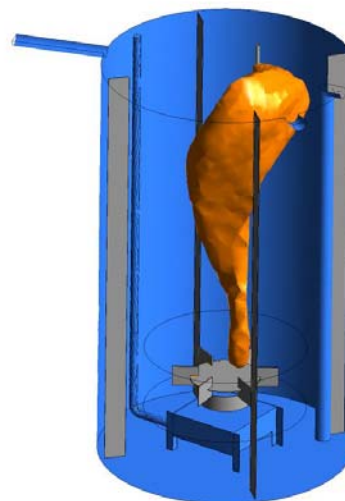


Figure 15: PNCr Vessel: Acid isosurface for recommended inlet location

CASE STUDY 2 – COAL-FIRED AIR HEATER

PNCR utilises rotary dryers for ore drying at the front end of the plant. Of the three dryers, two are coal fired and the other operates on gas.

Inside the coal-fired units, a rotary feeder throws the feed coal onto a grate conveyor located at the bottom. The grate conveyor discharges the spent material (ash) into a hopper. Coal situated on the grate is burnt using primary air injected below the grate. Figure 16 shows the actual combustion at the surface of the coal bed. Hot combustion gases and entrained solids flow from the grate to the top of the furnace, where they enter a duct connecting to the rotary dryer. A schematic of the furnace combustion system is shown in Figure 17.



Figure 16: Coal becoming entrained in primary air

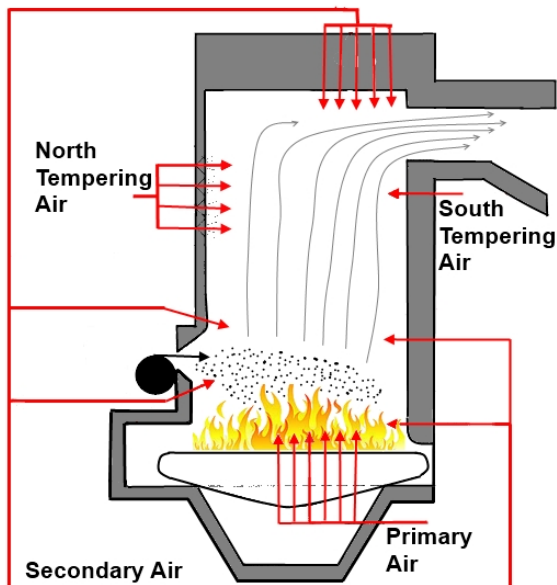


Figure 17: Air heater air injection points

The air heater under consideration at PNCR uses coal particles with sizing below 3mm. As a direct result of the small particle sizing, fine particles become entrained in the primary air flow. These particles continue to travel through the furnace and ducting where some of the particles stick to solid surfaces or drop out due to gravitational settling. The rest of the particles continue through to the rotary dryer.

The accretion behaviour of particulates inside the furnace and ducting was not clearly understood and the removal of the accretion build-up was identified by operations as a hazardous activity, due to instability of the accretion layer on the ceiling of the ducting.

CFD was identified as a valuable tool to help understand the accretion behaviour. Developing an operating regime to minimise the amount of build-up in the hazardous regions of the ducting was also a key consideration in the analysis.

Understanding the Existing Accretion Behaviour

A CFD analysis of the existing air heater and duct arrangement was performed in ANSYS CFX. The domain of interest including the furnace freeboard and connecting hot-gas ductwork up to the point at which it connected to the dryer hood. The focus of the CFD model was on the entrained solid-phase and the analysis was performed under isothermal conditions (with a gas temperature of 1035°C). An analysis of the coal combustion or related processes was not required, greatly reducing the computational effort.

The existing operating conditions were used as a base case for this analysis. A total of 25.9 m³/s of air was injected into the coal burner through the; primary, secondary, and tempering air injection points, apportioned as shown in Table 4.

| Existing Operating Conditions | | |
|---|-------------------|-------|
| Item | Units | Value |
| Primary Air Flow Input Runs 1-4 | m ³ /s | 13 |
| Secondary Flow Input Runs 1-4 | m ³ /s | 5 |
| Tempering Air via North Side Nozzles Runs 1-4 | m ³ /s | 7 |
| Tempering Air via South Side Nozzles Runs 1-4 | m ³ /s | 0.9 |
| Isothermal Temperature | °C | 1035 |

Table 4: Base Case Operating Conditions

Three different particle sizes were analysed; 1µm, 50 µm, and 500 µm. As a worst case analysis, all particle-wall contact events were assumed to result in adhesion of the particle to the wall. The particle wall mass flow densities were plotted to determine where the particles were likely to contact walls and potentially stick.

Results

The general nature of the gas flow in the air heater is shown in Figure 18 and Figure 19. From the base case CFD analysis, it was seen that the particles impact locations are identical to that found during operation. Build-up located on the roof of the duct entrance is the major region of concern for accretion formation because of the hazardous nature of accretion removal in this area. A contour plot showing a typical particle wall mass flow densities distribution is shown in Figure 20.

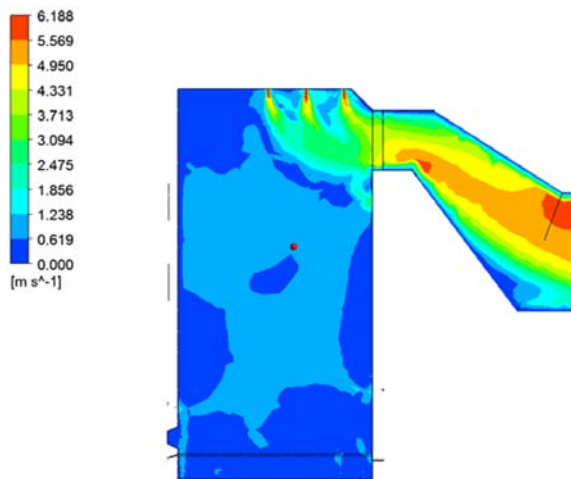


Figure 18: Base case (air velocity contour)

All three particle sizes show potential accretion in the regions of concern. Not surprisingly, it was noticeable that a higher percentage of the larger particles (500 μm) collected on the walls compared to the finer (1 μm) particles that carrying through the fluid domain into the dryer.

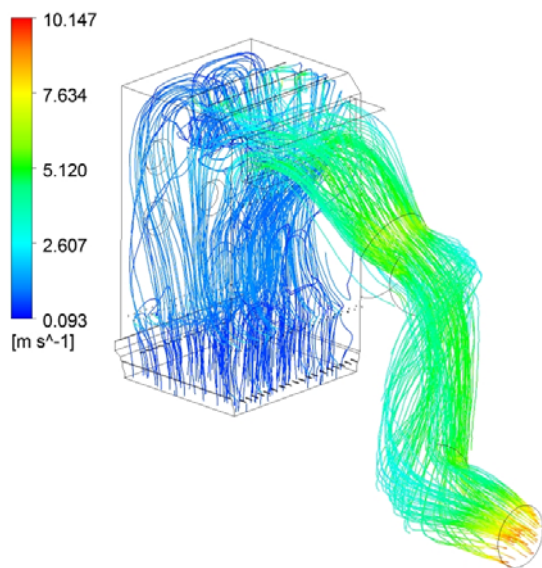


Figure 19: Particle Streamlines 1 μm (velocity) collect on walls)

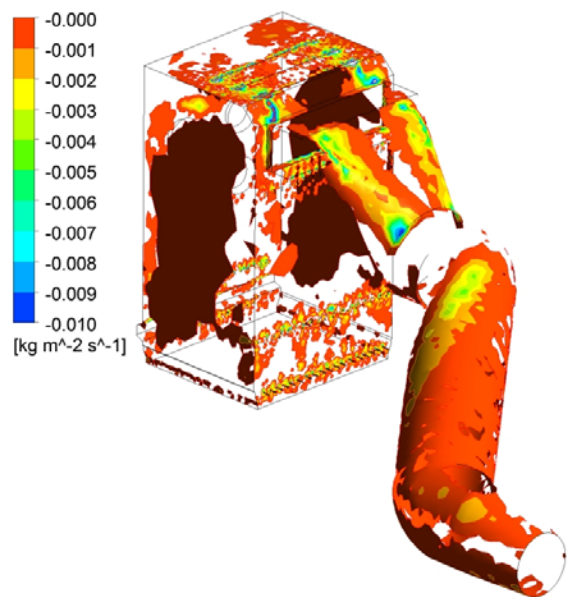


Figure 20: Mass flow density (50 μm particles)

Variations to Operating Conditions

Fourteen different CFD simulations were conducted to predict the flow patterns and particle trajectories during dissimilar operating regimes. Of the fourteen simulations, six involved simple design modifications to the furnace with the aim of minimising accretion in regions of the duct where removal is hazardous.

In simulating different operating conditions, an analysis was performed to understand the effect of blocked roof nozzles. When completely blocked, the secondary air entering the furnace through the lower sections must be increased to maintain the same overall aeration. In this mode of operation, it was found that 67% of the 50 μm particles impact the walls - corresponding to an increase of 10.6% from the standard operation.

| Simulation Condition | Percentage of Particles Impacting Walls |
|--|---|
| Roof nozzles completely blocked from accretion build-up | 67 % |
| Increased air through roof nozzles to prevent accretion build up | 65 % |
| More South tempering air and less North tempering air (0.5kg/s) | 57 % |

Table 5 – Variations to operating conditions

Variations to the flow entering the system did not improve flow around the duct entrance. However, having completely blocked roof nozzles showed a significant increase in the number of particles contacting the walls of the duct. The gas-flow pattern in the air heater under these conditions is shown in Figure 21.

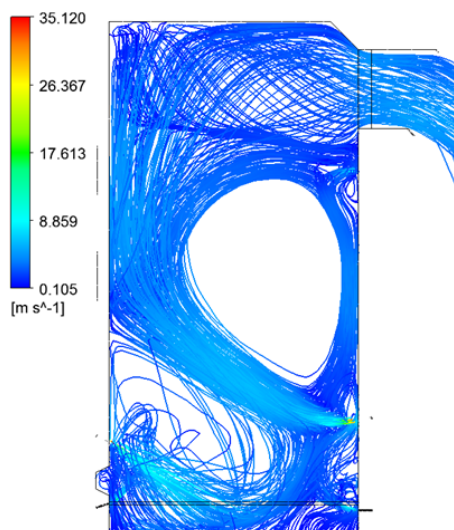


Figure 21: Stronger recirculation within the air-heater caused by blocked roof nozzles.

Design Modifications

For comparison purposes, all simulations involving design modifications (listed Table 6) used 50 μm particles. Injecting additional air with the aim of creating a particle-free boundary layer on the roof of the ducting was tested. Improvement in the transition between the coal burner and the ducting was also examined. The final analyses focussed on increasing the entrance cross-sectional area of the duct and rounding edges to create a smooth transition.

| Simulation Condition | Percentage of Particles Impacting Walls |
|--|---|
| Additional air to create boundary layer on roof of duct | 61 % |
| 10 additional inlets on duct roof to create boundary layer | 56 % |
| 49 additional inlets on duct roof to create boundary layer | 55 % |
| 49 additional inlets on duct roof, with increased additional south tempering air | 60 % |
| Smoothed internal walls entering duct to aid in flow transition | 46 % |
| Enlarged duct entrance | 56 % |

Table 6 – Design modifications

Additional nozzles in the roof of the duct did not show sufficient improvement to warrant design modifications. Using a smoother entrance to the duct showed small improvements to the flow pattern with less particles sticking to the walls of the duct.

Enlargement of the cross-section of the duct entrance by a factor of 50% reduced the flow speeds entering the duct (Figure 22). The smoother entrance into the duct results in a reduction in the number of particles impacting the internal roof of the duct by approximately 25% when compared to the standard operating condition. Results

from this analysis showed that particles could still potentially stick to the walls of the duct further downstream.

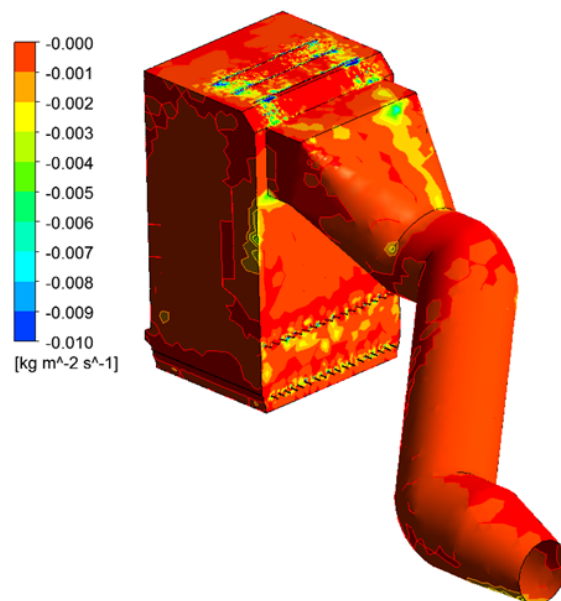


Figure 22: Mass flow density - enlarged duct entrance

Conclusions and Recommendations

Two case studies have been presented in which very complicated physical problems have been simulated simply using CFD. While omission and/or simplification of the relevant physics leads to computational models that are neither universally applicable nor phenomenologically complete, the results in both cases have provided valuable insight ultimately yielding the solution to significant industrial problems.

ACKNOWLEDGEMENTS

The authors would like to thank PNCr for their assistance in the preparation of this paper and for the permission for its publication.

REFERENCES

- Atiema-Obeng, V., Paul, E. and Kresta, S., (2004), “*Handbook of Industrial Mixing: Science and Practice*”, John Wiley & Sons
- Oldshue, J., (1983), “*Fluid Mixing Technology*”, McGraw-Hill Publications Co., New York, N.Y.
- Weetman, R and Salzman, R., (1981), “Impact of Side Flow on Mixing Impellers”, *Chemical Engineering Progress*, v77, n6, 71-75